The Aeronautical Journal (2022), **126**, pp. 1242–1264
doi:10.1017/aer.2022.32

REGULAR PAPER
2022 ISABE Conference Paper

Multidisciplinary conceptual design for a hybrid-electric commuter aircraft

C.P. Nasoulis*, V.G. Gkoutzamanis and A.I. Kalfas

Laboratory of Fluid Mechanics and Turbomachinery, Department of Mechanical Engineering, Aristotle University of Thessaloniki, Thessaloniki, Greece
*Corresponding author. Email: nasoulic@meng.auth.gr

Received: 18 October 2021; **Revised:** 23 February 2022; **Accepted:** 9 March 2022

Keywords: Component positioning; Conceptual design; Design space exploration; Electrified propulsion; Hybrid-electric aircraft; Structural optimisation

Abstract

The electrification of the commuter aircraft is instrumental in the development of novel propulsion systems. The scope of this work aims to explore the design space of a parallel hybrid-electric configuration with an entry into service date of 2030 and beyond and determine the impact of other disciplines on conceptual design, such as components positioning, aircraft stability and structural integrity. Three levels of conceptual sizing are applied and linked with a parametric aircraft geometry tool, to generate the aircraft's geometry and position the components. Subsequently, the structural optimisation of the wing box is performed, providing the centre of gravity of the components placed inside the wing, that minimise the induced stresses. Furthermore, the stability and trim analysis follow, with the former being highly affected by the positioning of components. Results are compared to a similar aircraft with entry into service technology of 2014 and it is indicated that in terms of block fuel reduction the total electrification benefit increases with the increase of degree of hybridisation, if aircraft mass is kept constant. On the other hand, if battery specific energy is kept constant, similar block fuel reduction is possible with lower hybridisation degrees. The potential for improvement in terms of carbon dioxide emissions and block fuel reduction ranges from 15.73% to 21.44% compared to the conventional aircraft, for levels of battery specific energy of 0.92 and 1.14 kWh/kg respectively. Finally, the component positioning evaluation indicates a maximum weight limitation of 240 kg for the addition of an aft boundary layer ingestion fan to a tube and wing aircraft configuration, without compromising the aircraft static stability.

Nomenclature

Abbreviations

BLI	Boundary Layer Ingestion
DEP	Distributed Electric Propulsion
DoH	Degree of Hybridisation
EIS	Entry Into Service
KPI	Key Performance Indicators
TLAR	Top-Level Aircraft Requirements
TRL	Technology Readiness Level

Variables

AR	Aspect Ratio (-)
$\bar{c}$	mean aerodynamic chord (m)

This paper is a version of a presentation due to be given at the 2022 ISABE Conference

https://doi.org/10.1017/aer.2022.32 Published online by Cambridge University Press

C_i	coefficient (-)
d	distance (m)
e	Oswald parameter (-)
E	endurance time (h)
E_{sb}	batteries specific energy ($\frac{Wh}{kg}$)
G	glide parameter (-)
H_p	degree of hybridisation (-)
M	mach number (-)
$MTOM$	Maximum Take-off Mass (kg)
OEM	Operating Empty Mass (kg)
P	power (kW)
p	specific power (kW/kg)
q	dynamic head (Pa)
S	reference area (m^2)
T	thrust (N)
TOP	Take-Off Parameter (-)
V	velocity (m/s)
W	mass (kg)
$\bar{X}$	longitudinal location divided by $\bar{c}$ (-)
z_E	vertical engine location (m)

Greek symbol

δ_f	flap deflection (deg)
η_i	efficiency (-)
σ	density ratio (-)

Subscripts

acw	aerodynamic chord of wing
$b2s$	batteries to shaft
CoG	centre of gravity
D_0	parasite drag
D	drag
fus	fuselage
h	horizontal tail
IE	Installed Engines
L	lift
LG	Landing Gear
m	moment
np	neutral point
p	propeller
to	take-off
VT	Vertical Tail
W	wing

1.0 Introduction

Moving forward to the current decade, novel propulsion architectures will emerge to comply with the emission and noise regulations posed by aviation administrations around the globe. According to European Aviation Safety Agency – EASA, 3% of total carbon emissions is generated by air transportation. In addition, it is estimated that the total number of flights in Europe will increase by 42% until 2040, compared to 2017, leading to an increment of 21% in respective carbon-dioxide emissions [1]. To overcome this increase, alternative propulsion concepts are being investigated, one of them being the hybrid-electric propulsion. Considering the current technological maturity, the commuter aircraft class is an ideal electrification candidate. That is because battery technology, neither is, nor will be capable of covering energy and power requirements for aircraft with gross take-off mass of 25 tonnes and above

https://doi.org/10.1017/aer.2022.32 Published online by Cambridge University Press

in the foreseeable future [2]. While methodologies for conventional aircraft sizing are well-established, as seen in the work of Henderson et al. [3], aircraft hybridisation studies are still under the microscope. Thus it is necessary to determine the status and the level of fidelity of publicly available approaches and decide the way forward.

1.1 Review on conceptual design methods and state of the art

Most of the time, traditional conceptual sizing methods, i.e., Roskam [4], Raymer [5], Gudmundsson [6], Nicolai [7] etc., are modified to apply to hybrid-electric architectures and used by authors widely in the literature. A generic range equation is derived in the work of De Vries et al. [8], suitable for hybrid-electric propulsion systems, that can be applied under quasi-level flight conditions for constant power split. In the same direction Nam et al. [9], propose a more generalised method of aircraft sizing, applicable to aircraft consuming unconventional types of energy of any kind. It is a power-based method consisting of a generic propulsion system including consumable and non-consumable weight and energy sizing calculations.

In the work of Finger et al. [10], a comparison between two individual sizing methods for hybrid-electric architectures is conducted, to validate the accuracy of their tools. The first method, as described in Ref. [11] focuses on a Vertical Take-Off and Landing -VTOL general aviation aircraft, considering point performance and mission analysis for the sizing. An energy-based approach is applied to multi-discrete mission segments and the required energy per mission phase is calculated. For the second method [12], a similar energy-based approach is implemented for a transport aircraft, considering the aero-propulsive interaction of novel concepts like Distributed Electric Propulsion – DEP and Boundary Layer Ingestion – BLI. The scope of the comparison is to validate the general approach in hybrid-electric aircraft sizing. A first design space analysis is provided, given a set of Top-Level Aircraft Requirements – TLAR, and Key Performance Indicators – KPI, like the hybridisation degree, power-to-weight ratio, and wing loading, are determined. A conventional aircraft resembling the Dornier Do 228 is selected as means of verification. Both tools can simulate series, parallel and fully electric powertrain configurations, by re-matching the aircraft's mass to the target performance. The results of both models coincide within an error of 4%, proving the correct formulation of the hybrid-electric sizing case.

The work is expanded to the commuter class in the works of Orefice et al. [13] and Trainelli et al. [14], with both authors aiming to comply with the CS-23 [15]/FAR-23 [16] airworthiness certification in their study. The former research examines the case of DEP for a 19-seater aircraft and estimates the operating empty mass at component level. The latter research proposes a procedure for sizing propeller-driven aircraft consisting of a mass breakdown and power estimation per mission phase using a time-marching algorithm that performs the full sizing. Additionally, in the work of Kruger et al. [17], a sizing and optimisation framework for hybrid-electric aircraft is presented, considering DEP, again for a 19-seater aircraft, able to capture trade-offs of electrification and aims to minimise the energy cost per seat-mile. Moreover, the work of Fefermann et al. [18] examines a 19-seater, tri-prop aircraft with an electric aft fan, aiming at the CS-25 [19] airworthiness certification. Two variants are explored, namely the electrical booster and the electrical booster with exchangeable battery pack, that are compared to the reference aircraft (a Beechcraft 1900D) and to an extrapolated reference aircraft design with an Entry Into Service – EIS date of 2030, to be comparable to the EIS of the hybrids. Trade-off between range and fuel saving are evident, indicating that the lower the range the higher the fuel saving, compared to the reference aircraft. Additionally, it is observed that a minimum of 0.5 kWh/kg battery specific energy is required to justify the electrification, compared to the conventional aircraft. Finally, the work of Gkoutzamanis et al. [20] studies a tri-fan light aircraft with an aft BLI fan and examines airworthiness standards for the design. Results indicate that compromises in the TLAR must be made to comply with the CS-23 standards, for the hybrid-electric turbofan. According to their review in energy storage State of the Art – SoA, the specific energy of batteries neither is, nor will be available by 2030 to satisfy the selected TLAR of the turbofan, thus the design requirements must be revised.

When examining large aircraft, the work of Gesell et al. [21] indicates a potential reduction of 21% in the block fuel from a parallel-hybrid ATR 72 with electric power supplied only at Take-Off and Climb

https://doi.org/10.1017/aer.2022.32 Published online by Cambridge University Press

phases, compared to the conventional ATR 72, with battery specific energy of 0.2 kWh/kg. Similar batteries SoA is assumed in the work of Juretzko et al. [22], where a Dornier Do 228 is retrofitted, that is capable of performing Take-Off and Climb with electric power only, while batteries maintain charge in cruise. The payload is reduced to maintain the maximum take-off weight, as a penalty of the addition of the electric powertrain. Compared to the conventional Do 228, the range of the retrofit is reduced by 37%, indicating that the retrofit cannot perform as the baseline, with the current battery SoA. Finally, more promising indications are presented in the work of Wall et al. [23], where a Cirrus SR20 is retrofitted, with simulation suggesting a fuel saving of 15.6%, compared to the conventional aircraft.

From the aircraft sizing review, it is observed that most of the approaches focus on batteries and fuel weight estimation and hybrid-electric powertrain sizing and performance, without examining other disciplines, i.e., component positioning, aircraft stability and structural evaluation. In a commuter aircraft, space is a limiting factor in terms of positioning and energy storage space availability. Moreover, the CS-23 airworthiness certification poses a mass limit of 8,618 kg [15], that complicates aircraft electrification, as the additional weight penalty of the electric powertrain is substantial. In a conventional aircraft, fuel is stored inside the wing-box and has a minor impact on the overall stability. Furthermore, it is depleted during the mission, thus reducing the aircraft's weight and structural loads. However, in a hybrid-electric aircraft, where batteries are present, the total mass of the aircraft is greater, increasing the structural loads. In addition, the positioning of the batteries is important, as it is a considerable amount of weight, thus affecting the overall stability of the aircraft. Given the above, it is necessary to include the positioning and stability disciplines in the aircraft sizing process and address the challenges in the design. All things considered, the present work aims to explore the design space for a 19-seat hybrid-electric commuter aircraft, with an EIS date of 2030. At first, the sizing methodology is presented, expanding up to a third level of refinement. Subsequently, an automated procedure for the geometry generation of the aircraft is explained, followed by the structural optimisation of the wing-box. In addition, the positioning of the components occurs, and static stability and trim analysis calculations are showcased. All the above are included in a single framework, forming a multidisciplinary environment that is capable to connect to additional — more detailed — sizing modules for different aircraft components. Results explore the design space for the parallel hybrid-electric configuration with electric power supplied at all mission phases. Additionally, the potential for block fuel reduction of the design, compared to a conventional configuration with EIS date of 2014, is established while exploring different technological advancements. Finally, the impact of the positioning of components and structural optimisation on the Centre of Gravity – CoG and stability of a designed aircraft is discussed.

1.2 State of the art and challenges in electrical machines

The SoA of energy storage is reviewed in the work of Gkoutzamanis et al. [20]. However, energy storage is not the sole driver in hybrid-electric aircraft design. The Technology Readiness Level – TRL of electrical machines will also determine the feasibility of a hybrid-electric design. Considering the work in Ref. [24], the specific power of electrical components will determine the overall weight of the electrical powertrain. Table 1 indicates the research that is under progress globally and is publicly available through several references. Applicability in the small aircraft is again commented along with the various concerns around these components of the powertrain.

Most technologies currently under research, have lower specific power which makes them impractical for the case of the 19-passenger aircraft. Bodson et al. [25], consider a Hybrid Electric Propulsion – HEP system that transmits the power from the generator directly to electrical motors, without conversion in-between. The validation of their work is performed at a low-power test bench, and results indicate that this configuration can be scaled-up for commercial air-transportation use successfully.

Furthermore, because CS-23 imposes significant weight limits, one of the primary goals of design is to have a powertrain as lightweight as possible. One potential solution is to match the propeller and motor to eliminate the need for gearbox, while the motor is operating at low rpm. The challenge at this point is to ensure that the speed of the motor shaft is equal to the speed of propellers. This implies that

https://doi.org/10.1017/aer.2022.32 Published online by Cambridge University Press

Table 1. *Technology Readiness Level – TRL and applicability of electrical propulsion systems (Refs. [26]– [35])*

Name	Efficiency	Specific power (kW/kg)	Rated power (kW)	TRL [36]	Applicability
Axial flux machine EMRAX 348, MAHEPA Project [26]	0.92	10	420	9	High Specific Power, Applicable to Commuter aircraft, EASA certified
Permanent Magnet Synchronous Machine, NASA X-57 – Joby Aviation [27]	n/a	3	60	6-7	Applicable to Commuter aircraft via DEP
SP70D, e-Flyer 2 [28]	0.95	5.22	70	6-7	Applicable to Commuter via DEP
Direct Drive Permanent Magnet machine, SP260D/D-A, Extra330LE and Eviation Alice [28]	0.95	5.22	260	6-7	Applicable to Commuter aircraft via DEP
Direct Drive Permanent Magnet Machine, SP200D, CityAirbus [28]	0.95	5.22	204	6-7	Applicable to Commuter aircraft via DEP
Magnix, Eviation Alice, De Havilland DHC-2 Beaver Seaplane [29]	0.93	5.5	280/560	6-7	Applicable to Commuter aircraft
SP2000D, Airbus E-Fan X [28]	n/a	n/a	2,000	6-7	Applicable in Commuter aircraft through scalable technology
Switched Reluctance Motor, NASA Boeing SUGAR Volt [30]	0.93	3-5	n/a	3-4	Applicable in Commuter aircraft through scalable technology
High efficiency MW motor, STARC-ABL, Partially Superconducting WFSM, NASA Glenn Research Centre [31]	0.98	16	1,400	3-4	Applicable in Commuter aircraft through scalable technology
Induction Motor, Ohio State University [32]	0.96	13	2,700	4-5	Applicable in Commuter aircraft through scalable technology
Wound field synchronous machine, Honeywell Future Aerospace Application [33]	n/a	7.9	1,000	3-4	Applicable in Commuter aircraft through scalable technology
Air core Permanent Magnet machine, University of Illinois [34]	0.96	13	1,000	3-4	Applicable in Commuter aircraft through scalable technology
High Speed HTS Generator, General Electric – Air Force Research Labs (AFRL) [35]	0.97	13	1,300	3-4	Applicable in Commuter aircraft through scalable technology

https://doi.org/10.1017/aer.2022.32 Published online by Cambridge University Press

Table 2. *Top-level aircraft requirements*

Accomodation	19 seats
Weight per passenger (baggage incl.)	100 kg
Crew	1
Take-Off Field Length (TOFL)	<800 m (@MTOM, SL, ISA)
Landing field length	<780 m (@MLM, SL, ISA)
Climb (97% MTOM @SL, ISA, OEI)	≥3 m/s
Climb (97% MTOM @SL, ISA, AEO)	≥10.9 m/s
Approach speed	≤62 m/s
Loiter endurance	30 min
Service ceiling (AEO)	FL100
Cruise mach number @97% MTOM	0.3
Maximum cruise mach number	0.35
Range	400 nm
Reserves	100 nm
Certification as to new level 4 CS-23/FAR-23	≤8,618 kg

the motor must be designed in such a way to withstand torque and thrust loadings, as well as structural and vibration loads emanating from the propeller rotation. The requirement for high current densities implies that the thermal management system is the key enabler for the development of such machines. Lastly, to attain full entitlement of new machine architectures, advanced manufacturing techniques such as to build slot-less windings, composite structures and superconducting coil assemblies need to be purchased.

2.0 Methodology

2.1 Top-level aircraft requirements

In order to initiate the design process, the Top-Level Aircraft Requirements – TLAR must be defined, that are selected according to the mission type and aircraft design and can be modified if the design constraints are not met. In Table 2, the design case TLAR are presented, selected to be similar to those in the work of Romano et al. [37], as they are based on market related scenarios. The selected reference aircraft is a conventional twin-turboprop, equipped with two engines similar to PT6A-67D Pratt & Whitney [38] and an EIS date of 2014. On the other hand, the examined hybrid-electric configuration is a parallel-hybrid, twin-turboprop aircraft with a potential EIS of 2030+. Both aircraft were sized within the proposed framework using a simple mission profile, consisting of five discrete segments: 1. Taxi and Take-Off, 2. Climb, 3. Cruise, 4. Descend and Loiter, 5. Approach, Landing and Taxi-back, as shown in Fig. 1.

2.2 Aircraft sizing

To calculate the maximum take-off mass, the operating empty mass and the required amount of fuel and batteries, the methodology that is followed is based on that proposed by Raymer [5], modified accordingly to fit the hybrid-electric architecture. The aforementioned masses are described as fractions of the maximum take-off mass in Equation (1), which is solved iteratively to calculate the maximum take-off weight. The operational empty mass fraction is estimated using historical data for the first two levels of sizing, as described in Equation (2). Parameters A, C, K_{VS}, α_0, α_1 and $c_1 - c_5$ are derived from tabulated data for twin-turboprop aircraft [5]. Since the regression curves that these equations describe are derived for conventional aircraft, the additional weight of the electric powertrain is estimated and

https://doi.org/10.1017/aer.2022.32 Published online by Cambridge University Press

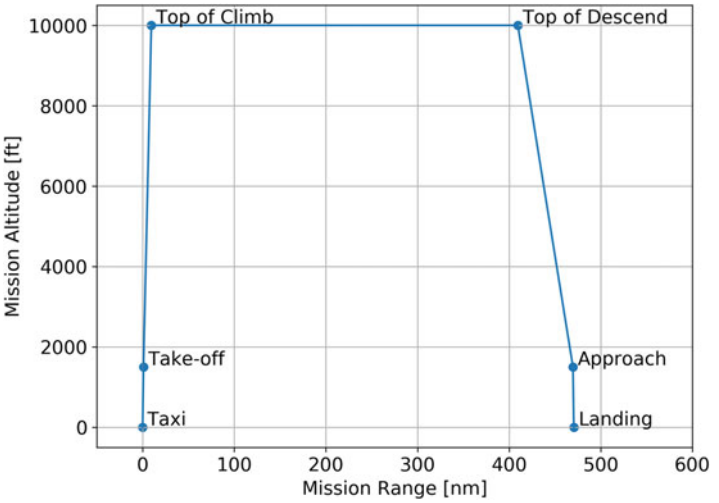

Figure 1. *Design mission.*

included in the empty weight calculation in a forward step.

$$MTOM = \frac{W_{crew} + W_{payload}}{1 - \frac{W_{empty}}{MTOM} - \frac{W_{fuel}}{MTOM} - \frac{W_{batteries}}{MTOM}} \tag{1}$$

$$\frac{W_{empty}}{MTOM} = \left(A \cdot MTOM^{C} \cdot K_{VS}, a_0 + a_1 \cdot MTOM^{c_1} \cdot AR^{c_2} \cdot \left(\frac{P}{W}\right)^{c_3} \cdot \left(\frac{W}{S}\right)^{c_4} \cdot V_{\max}^{c_5} \right) \tag{2}$$

Fuel and battery mass fractions are calculated for each discrete mission segment, considering the Degree of Hybridisation – DoH in terms of power, as it is described in Equation (3). According to this definition, P_{el} is the continuous electrical power of the electric motor and P_{gt} is the power provided by the gas turbine. The Degree of Hybridisation can receive any value between 0 and 1, with 0 representing the conventional aircraft and 1 the pure electric. For the parallel hybrid configuration, the total thrust can be divided into thrust produced by the electric motor and gas turbine respectively. Climb, cruise and loiter can be considered steady level flight segments; climb is a superposition of level flight and climb gradient. This consideration poses a direct relationship between Lift and Weight and Thrust and Drag, derived from the free-body diagram, that allows the substitution of T/W ratio with the inverse L/D ratio. Hence, H_p can be multiplied with Drag to account for the electrically produced thrust. Therefore, the required battery mass fractions are calculated using Equations (4)–(6).

$$H_p = \frac{P_{el}}{P_{gt} + P_{el}} \tag{3}$$

$$\left.\frac{W_{batteries}}{MTOM}\right|_{loiter} = \frac{E \cdot V_{loiter} \cdot g}{3.6 \cdot E_{sb} \cdot \eta_p \cdot \eta_{b2s} \cdot \left.\frac{L}{D}\right|_{loiter} \cdot \frac{1}{H_p}} \tag{4}$$

$$\left.\frac{W_{batteries}}{MTOM}\right|_{cruise} = \frac{R \cdot g}{3.6 \cdot E_{sb} \cdot \eta_p \cdot \eta_{b2s} \cdot \left.\frac{L}{D}\right|_{cruise} \cdot \frac{1}{H_p}} \tag{5}$$

$$\left.\frac{W_{batteries}}{MTOM}\right|_{climb} = \frac{h \cdot g}{3.6 \cdot E_{sb} \cdot \eta_p \cdot \eta_{b2s} \cdot V_v} * \left[V_v + \frac{V_{climb}}{\left.\frac{L}{D}\right|_{climb} \cdot \frac{1}{H_p}} \right] \tag{6}$$

https://doi.org/10.1017/aer.2022.32 Published online by Cambridge University Press

Table 3. *Tabulated fuel mass fractions* $\frac{W_i}{W_{i-1}}$ *[5].*

Level 1		Level 2	
Take-off	0.97	Take-off	0.97–0.99
Climb	0.985	Climb	1.0065–0.0325*M
Loiter	0.995	Landing	0.99–0.995
		Taxi	0.992–0.997

The fuel mass fraction is calculated using Breguet's equation for cruise and loiter as shown in Equations (7)–(8), whereas fixed ratios are selected from tabulated data for all other segments, as shown in Table 3, and are used in Equation (9). Additionally, 6% trapped fuel after landing is also considered in Equation (9).

$$\left.\frac{W_i}{W_{i-1}}\right|_{cruise} = exp\left[\frac{-R \cdot SFC_{cruise}}{V_{cruise} \cdot \left.\frac{L}{D}\right|_{cruise} \cdot \frac{1}{1-H_p}}\right] \tag{7}$$

$$\left.\frac{W_i}{W_{i-1}}\right|_{loiter} = exp\left[\frac{-E \cdot SFC_{loiter}}{\left.\frac{L}{D}\right|_{loiter} \cdot \frac{1}{1-H_p}}\right] \tag{8}$$

$$\frac{W_f}{MTOM} = 1.06 \cdot \left(1 - \prod_{i=1}^{n} \frac{W_i}{W_{i-1}}\right) \tag{9}$$

$$\frac{P}{W} = \max\left(0.33, 0.016 \cdot V_{\max}^{0.5}, \left.\frac{T}{W}\right|_{take-off} \cdot g \cdot \frac{V_{take-off}}{\eta_p}\right) \tag{10}$$

$$\frac{L}{D} = \frac{1}{\frac{4 \cdot C_{D0}}{W/S} + \frac{W}{S} \cdot \frac{1}{q \cdot \pi \cdot AR \cdot e}} \tag{11}$$

The proposed aircraft sizing method is an in-house tool developed in Python programming language and is connected to OpenVSP [39] to generate the aircraft 3D sketch with a geometry generator, that has been developed for the purposes of this work. The resulting 3D sketch provides the required information (i.e., exposed, and wetted areas and individual component volumes) to proceed to the final level of sizing. In addition, this information is imported to the Aerodynamics module of the proposed framework, that calculates the parasite drag coefficient, using the parasite drag component build-up method. Finally, the centre of gravity vector for each component is extracted and will be used in the stability and control modules.

In the second sizing level, aircraft power loading is calculated using Equation (10) and L/D is calculated from the wing loading at each segment, using Equation (11). The aircraft wing loading is calculated for each mission phase according to the Top-Level Aircraft Requirements and the mission profile definition. Then, the actual wing loading is calculated for each phase, considering the change in aircraft mass throughout the mission. The more refined estimation of maximum take-off weight allows for a more accurate estimation of the dimensions for the fuselage, wing and empennage, that will lead in the final estimation of the aircraft empty mass. A component build-up method is deployed that examined each aircraft part an performs the mass estimation. Additionally, the weight of electrical components is included in this step, using the mass estimation method proposed by Teichel et al. [40]. It includes the mass estimation of electrical motors/generators, inverters, cooling components, gearbox, rectifiers, and cables. For electrical motors with continuous power less than 500 kW, a new mass estimation is introduced that is derived from data provided by EMRAX [26], considering continuous power ranging from 188 to 348 kW. The equations used to estimate the components mass (i.e., fuselage, wing, empennage,

https://doi.org/10.1017/aer.2022.32 Published online by Cambridge University Press

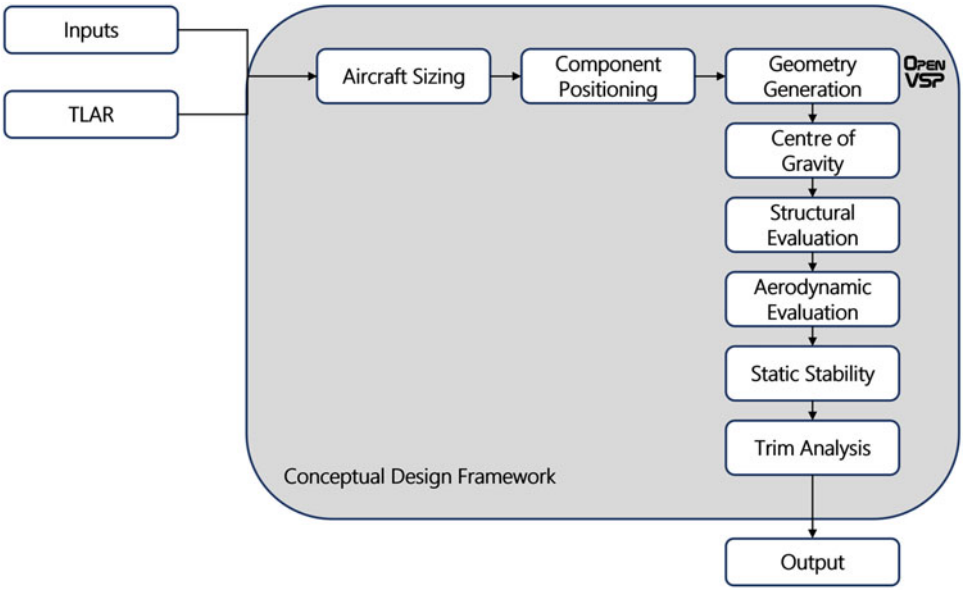

Figure 2. *Overall computational pipeline for the proposed framework.*

etc.) can be found in Refs. [41], [42] and in chapter 15 of Ref. [5]. For the sake of brevity, only the build-up of the operating empty mass is presented in Equation (12). The weight of avionics, furniture, consoles etc., is symbolised as W_{else} and is considered to be 17% of the maximum take-off mass, as proposed in Ref. [5].

$$OEM = W_W + W_{fus} + W_h + W_{VT} + W_{LG} + W_{IE} + W_{EPS} + W_{else} \tag{12}$$

The weight component build-up method qualifies as the third — and final — level of sizing. In this way, the impact of aircraft dimensions on the maximum take-off mass is captured. At each iteration, a new aircraft is sized, new dimensions are extracted, and an updated operating empty mass is calculated. Thus, the final maximum take-off mass is calculated, considering the actual dimensions of the design. Subsequently, the proposed design process continues with the other framework modules, namely Aerodynamics, Structural evaluation, Positioning, Centre of Mass and Stability, as shown in Fig. 2. In the Aerodynamics module, apart from the drag calculation, the aircraft drag polar is extracted as well. Additionally, in the structure model, the structural optimisation of the wing-box using a mixed-fidelity approach is performed and finally, the impact of component positioning on the aircraft centre of mass and static stability is evaluated. The output of all modules is thoroughly discussed in the results section.

2.3 Assumptions

The most important assumptions in the presented design process are listed below:

- Aircraft is fully loaded during the initial phases of the mission
- The operating empty mass is estimated from historical data in the beginning and the additional mass of the electric powertrain is considered in the third level of sizing
- "Rubber engines" are considered for the design evaluation, thus only the total power requirement is calculated

https://doi.org/10.1017/aer.2022.32 Published online by Cambridge University Press

Table 4. *Aircraft sizing code verification*

	Beechcraft 1900D [43]			Fairchild Dornier Do 228 [47]		
	Manufacturer	Prediction	Delta (%)	Manufacturer	Prediction	Delta (%)
MTOW (kg)	7,764	7,763	0.01	6,575	6,525	0.76
Empty (kg)	4,732	4,741	−0.19	3,900	3,871	0.74
Wing span (m)	17.64	19.98	−13.27	16.97	17.58	−3.59
Fuselage length (m)	17.62	16.29	7.55	16.56	14.9	10.02
Reference area (m^2)	28.8	36.96	−28.33	32	34.34	−7.31
	ATR 42-600 [48]			Fairchild Dornier Do 328 [49]		
	Manufacturer	Prediction	Delta (%)	Manufacturer	Prediction	Delta (%)
MTOW (kg)	18,600	19,362	−4.10	13,990	14,396	−2.90
Empty (kg)	11,550	11,623	−0.63	8,900	8,814	0.97
Wing span (m)	24.57	27.19	−10.66	20.98	22.74	−8.39
Fuselage length (m)	22.67	25.95	−14.47	21.23	22.31	−5.09
Reference area (m^2)	54.5	66.76	−22.50	40	47	−17.50

- Specific fuel consumption for cruise and loiter is selected from similar aircraft using PT6A-67D engines [43]
- Hot day ground conditions are considered
- The propeller efficiency for the discrete mission phases is estimated according to the work of Giannakakis et al. [44]
- The total electrical powertrain efficiency, from batteries to shaft ranges from 90% to 94% considering electrical machine efficiencies (92%–96%) from Table 1, inverter efficiency (99%) [45] and battery pack efficiency (99.1%) [46]
- Climb and approach speed are selected according to CS-23 [15]/FAR-23 [16] airworthiness certification
- A parallel hybrid-electric propulsion architecture is examined

3.0 Results and discussion

3.1 Model verification

The validity of the model has been verified using data from four different conventional aircraft as shown in Table 4. Data from aircraft manufacturers have been obtained and compared to the prediction of the proposed aircraft sizing tool. It is observed that the empty and maximum take-off weight prediction is within acceptable limits (< 5%) in all cases. When considering the aircraft dimensions (i.e., the fuselage length, span, and reference area), the prediction error increases. That is because, these parameters are subject to additional design selections that were assumed or calculated separately in the validation process. For example, both wing span and reference area depend on the wing loading selection. In this work, the wing loading is calculated for each mission segment, and the minimum value is selected for safety reasons. Additionally, the fuselage length is expected to change further down in the design process as part of the component positioning optimisation. Considering the above, the dimension deviation of the prediction compared to the manufacturer's data is considered within acceptable limits for a conceptual design tool.

https://doi.org/10.1017/aer.2022.32 Published online by Cambridge University Press

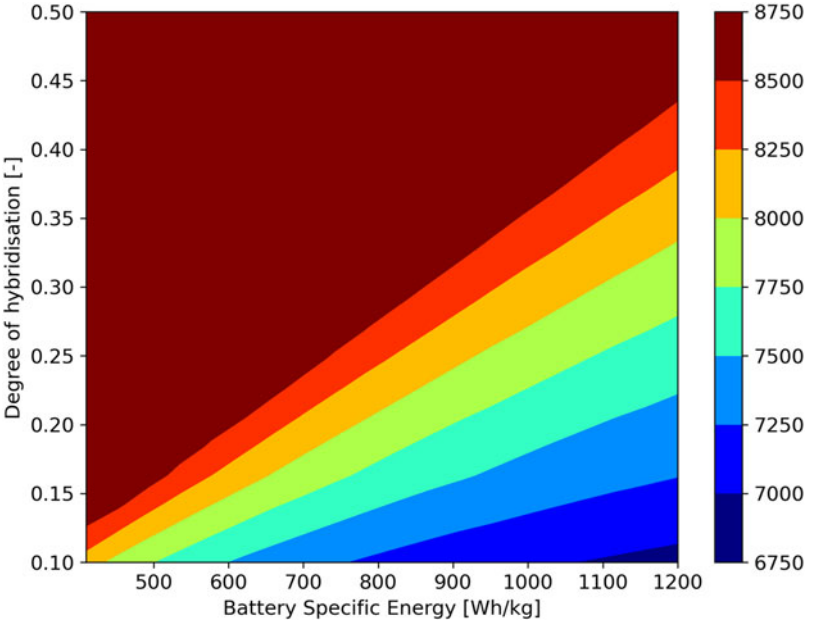

Figure 3. *Maximum take-off mass variation to degree of hybridisation and specific energy of batteries for service ceiling at 10,000 ft.*

3.2 Design space exploration

Using the framework described in the previous sections, a design space exploration is performed, using the third level of sizing, to determine the effect of the hybridisation degree and specific energy of the batteries on maximum take-off mass. Figures 3 and 4 show the variation of aircraft maximum take-off mass with respect to the specific energy of batteries and degree of hybridisation, for two different service ceilings, i.e., 10,000 and 25,000 ft. The mission range examined is 400 nm, plus 100 nm reserves and 30 minutes of loiter time, whereas the cruise speed is 195 kn. Pairs of values that result in a take-off mass $\geq$ 8,618 kg are filtered out of the graph, keeping in mind the CS-23/FAR-23 certification, which explains the constrained surfaces for the combination of low specific energy and high degree of hybridisation. It is evident that specific energy is the main driver of this design space exploration, especially in the lower values area, where the slope is greater. On the other hand, the effect of hybridisation degree on maximum take-off mass can be described as linear, but this can be also explained by the formulae presented in the previous section. Comparing the different service ceilings, it can be observed that the higher the altitude, the more the maximum take-off mass becomes. When flying at an altitude over 10,000 ft, oxygen must be carried to prevent hypoxia due to air being less dense at higher altitudes. Furthermore, a cabin pressurisation system must be added to the air conditioning system of the aircraft, that results in a weight penalty. This penalty is included in the operating empty mass in the present framework, which explains the increase in the maximum take-off mass, thus reducing the acceptable design space. In addition, increasing the top of climb, translates to additional fuel, that further increases the maximum take-off mass. Considering the operational aspects of a commuter aircraft and the mass limitation posed by the certification, a service ceiling of 10,000 ft is selected to reach an earlier EIS. Said that, it can be observed that the design space offers some realistic pairs when considering EIS of 2030+. It should be noted that with a compromise in the maximum range, the need for more energy-dense batteries will reduce, however this requires an area-based market analysis, which is out of the scope of this publication.

https://doi.org/10.1017/aer.2022.32 Published online by Cambridge University Press

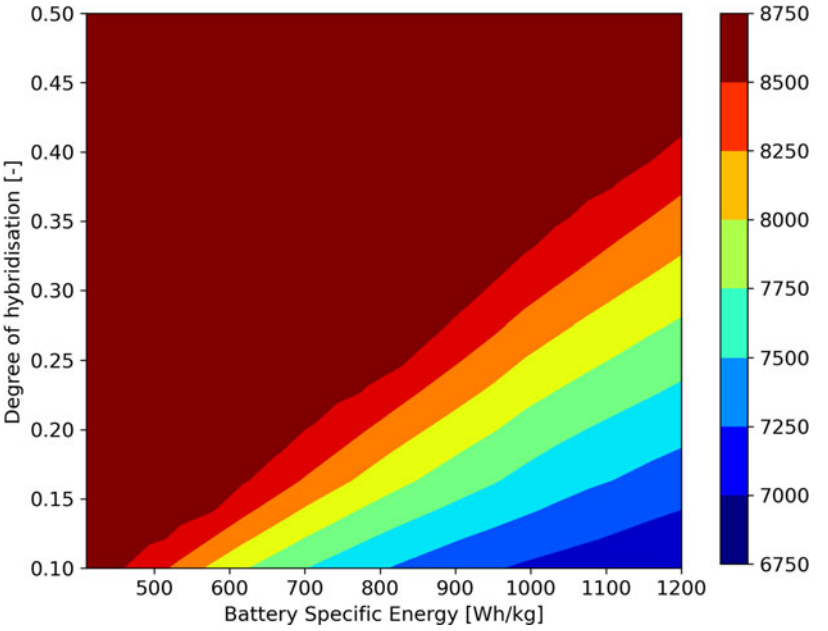

Figure 4. *Maximum take-off mass variation to degree of hybridisation and specific energy of batteries for service ceiling at 25,000 ft.*

3.3 Benefits of electrification

A comparison analysis follows between the reference aircraft and three different parallel hybrid-electric design cases with constant hybridisation degree throughout the mission. Four different H_p are selected, i.e., 30, 35, 40 and 50% per case, bringing up the total of compared cases to 12. Those cases are then examined for a selection of cruise ranges from 200 to 600 nm including additional 100 nm reserves, to determine the electrification benefit in terms of block fuel reduction, compared to the conventional aircraft, as shown in Table 5. The block fuel benefit for each hybrid-electric aircraft is calculated according to Equation (13) and is compared to the conventional aircraft, for each design range. For a fair comparison, all cases have the same maximum take-off mass of 8,600 kg. Since the maximum mass is fixed and the mission is pre-defined, batteries specific energy can change, to cover the specified mission. The required specific energy for each design case is summarised in Table 6.

$$\Delta m_{fuel} = \frac{m_{fuel,hybrid,i} - m_{fuel,conv.,i}}{m_{fuel,conv.,i}} \times 100 \tag{13}$$

All cases are sized within the proposed framework and aircraft characteristics are listed below:

Conventional EIS 2014 is the reference aircraft. The engines considered are similar to PT6A-67D from Pratt & Whitney, conventional materials are used for manufacturing and the propulsion system has two propellers with 80% efficiency at cruise. This aircraft is equipped with technology with EIS of 2014.

Hybrid EIS 2014 is the first examined case. It has the same engines as the *Conventional*, plus the electrical powertrain. Again, conventional materials are assumed, and the propellers have an efficiency of 80% at cruise. The overall efficiency of the electric system — from batteries to shaft — is considered 90%.

Hybrid EIS 2030+ *C* is a parallel hybrid with conservative estimation of the technology available for and aircraft with EIS of 2030+. Two hypothetical turboprop engines are used, assuming 10% less

https://doi.org/10.1017/aer.2022.32 Published online by Cambridge University Press

Table 5. *Block fuel reduction (%) compared to the conventional aircraft*

Range (nm)	H_p	200	300	400	500	600
Hybrid EIS 2014	0.3	−1.3	−5.2	−8.5	−11.2	−13.6
Hybrid EIS 2014	0.35	−3.5	−7.8	−11.4	−14.3	−16.9
Hybrid EIS 2014	0.4	−5.7	−10.5	−14.3	−17.4	−20.1
Hybrid EIS 2014	0.5	−10.2	−15.8	−20.1	−23.7	−26.7
Hybrid EIS 2030+ C	0.3	−4.4	−8.9	−12.5	−15.6	−18.2
Hybrid EIS 2030+ C	0.35	−6.4	−11.3	−15.2	−18.4	−21.1
Hybrid EIS 2030+ C	0.4	−8.4	−13.7	−17.8	−21.2	−24.0
Hybrid EIS 2030+ C	0.5	−12.5	−18.4	−23.1	−26.9	−30.0
Hybrid EIS 2030+ R	0.3	−8.4	−13.7	−17.8	−21.2	−24.1
Hybrid EIS 2030+ R	0.35	−10.2	−15.7	−20.1	−23.6	−26.6
Hybrid EIS 2030+ R	0.4	−11.9	−17.8	−22.3	−26.1	−29.1
Hybrid EIS 2030+ R	0.5	−15.4	−21.9	−26.9	−30.9	−34.3

Table 6. *Required battery specific energy (Wh/kg)*

Range (nm)	H_p	200	300	400	500	600
Hybrid EIS 2014	0.3	631	932	1,334	1,895	2,730
Hybrid EIS 2014	0.35	731	1,083	1,545	2,179	3,099
Hybrid EIS 2014	0.4	838	1,241	1,763	2,465	3,457
Hybrid EIS 2014	0.5	1,072	1,579	2,217	3,040	4,143
Hybrid EIS 2030+ C	0.3	597	867	1,212	1,668	2,298
Hybrid EIS 2030+ C	0.35	694	1,010	1,410	1,931	2,638
Hybrid EIS 2030+ C	0.4	796	1,160	1,614	2,199	2,975
Hybrid EIS 2030+ C	0.5	1,022	1,484	2,048	2,749	3,644
Hybrid EIS 2030+ R	0.3	378	521	684	872	1,091
Hybrid EIS 2030+ R	0.35	435	602	792	1,009	1,259
Hybrid EIS 2030+ R	0.4	495	687	903	1,148	1,429
Hybrid EIS 2030+ R	0.5	623	866	1,135	1,436	1,773

SFC than the reference case. The efficiency of the propellers at cruise remains 80%, whereas the overall electrical efficiency increases by 2% compared to the *Hybrid EIS* 2014 case.

Hybrid EIS 2030+ *R* is the most advanced variant of all. The EIS target is again 2030+, but some of the assumptions lean to the optimistic side. Two turboprop engines, with an SFC reduction of 20% compared to the *Hybrid EIS* 2014 are considered; a non-far-fetched assumption, according to the latest release of GE Aviation [50] about their new engine. The operating empty mass is reduced by 10%, considering the use of advanced materials and manufacturing in various aircraft components. The overall electrical efficiency is increased by 3%, compared to *Hybrid EIS* 2014 case, and the propeller efficiency at cruise is 83%.

Results for all cases with 35% degree of hybridisation are grouped in Fig. 5. It is observed that the benefit of electrification increases with the mission range, as cruise the longest mission phase. Furthermore, the radical improvement in technology, provides an even greater block fuel reduction, compared to the conventional case, as expected. However, since maximum take-off mass and operating empty mass are fixed, the battery specific energy varies, as shown in Table 6. As a result, less energy dense batteries are required if the efficiency of other components is also improved. Since battery specific energy $\geq$ 1,000 Wh/kg is still at experimental level [20], the whole powertrain system has to be improved, in order to have realistic expectations from aircraft electrification, with reference to 2014's technology.

https://doi.org/10.1017/aer.2022.32 Published online by Cambridge University Press

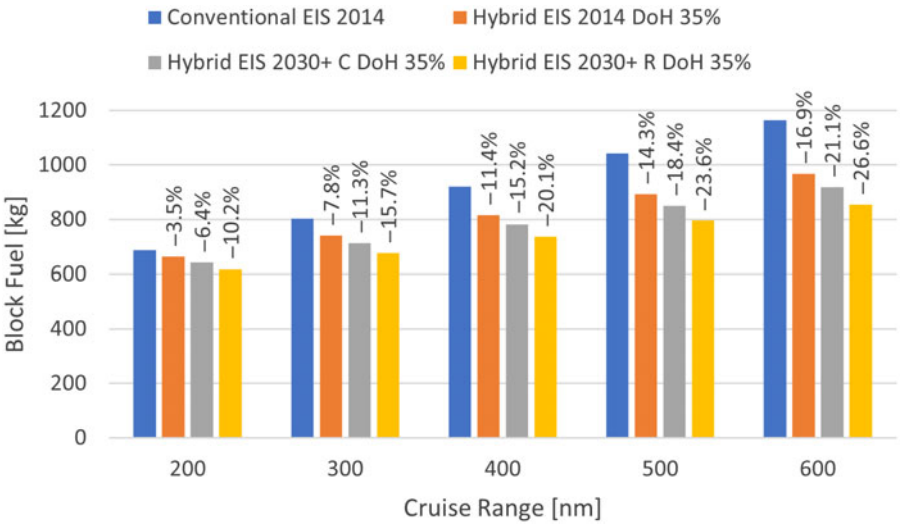

Figure 5. *Block fuel comparison of three different parallel hybrid-electic designs to a conventional aircraft (Cruise Speed 195 KTAS).*

In terms of emissions, CO_2 emissions are directly related to fuel consumption. For aviation fuel, 3.16 kg of CO_2 are emitted per kg of fuel burnt [1]. In the work of Nasoulis et al. [51] the environmental impact of both conventional and hybrid-electric aircraft with different propulsion configurations (i.e., turbofan and turboprop variants) is examined, considering a life cycle analysis for aircraft conceptual design. Additionally, both EU electricity mix and power from renewable sources are considered in the environmental impact single score assessment. It is observed that for a parallel-hybrid turboprop configuration with a hybridisation degree of 0.4 the impact of electricity production on the single score is 17.82% for the EU electricity mix, whereas the impact is 0.87% when renewables are used. Therefore, in the case of ground-based charging using renewable power sources the total operational CO_2 footprint of the hybrid-electric aircraft is reduced almost by the same amount as the block fuel. Considering charging only from renewable sources may be optimistic now, however it is an opportunity to unlock the full potential of electrification and replace fossil fuel-based energy with sustainable energy sources, both in aircraft and airport operations. For example, Schiphol airport in the Netherlands is committed to become a CO_2 neutral airport by 2030 [52]. This means that the aviation industry is currently investing in the upgrade of airport infrastructure towards a more sustainable mobility future.

3.4 Conceptual design summary

Sizing results for the examined aircraft are presented in Table 7. Considering the trends and remarks shown in the previous sections, three parallel hybrid-electric aircraft are sized, following the assumptions of the radical case presented in the previous section. Also, the conventional aircraft with EIS of 2014 is sized to serve as reference. Two different degrees of hybridisation and two different battery specific energies are tested. All cases comply with the CS-23/FAR-23 airworthiness certification, as the maximum take-off mass is less than 8,618 kg. *Hybrid* 1 assumes a radical improvement in specific energy (1,143 Wh/kg) which leads to a maximum take-off mass of 8,075 kg and 21.01% CO_2 and block fuel reduction. Since the specific energy selected in *Hybrid* 1 is very optimistic, *Hybrid* 2 is sized, with the same inputs apart from the battery specific energy. In *Hybrid* 2 the specific energy is considered 920 Wh/kg — still an optimistic value — than ensures that the maximum take-off mass will be within the certification limits. By decreasing the specific energy, the maximum take-off mass increases, leading

https://doi.org/10.1017/aer.2022.32 Published online by Cambridge University Press

Table 7. *Conceptual design summary*

Aircraft	Conventional	Hybrid 1	Hybrid 2	Hybrid 3
Propulsion system	2 × similar to PT6A-67D Turboprop Engines	2 × Hybrid Turboprop Engines	2 × Hybrid Turboprop Engines	2 × Hybrid Turboprop Engines
DoH (%)	0%	35%	35%	45%
Range (nm)	400	400	400	400
Reserves (nm)	100	100	100	100
Passengers	19	19	19	19
Specific energy of batteries	–	1,143	920	1,143
P/W (kW/kg)	0.266	0.2992	0.283	0.2831
Power (kW)	2 × 955 kW	2 × 1,208 kW	2 × 1,215 kW	2 × 1,215 kW
W/S (kg/m^2)	T.O. 183/Climb 177.5/Cruise 177/Loiter 165	T.O. 183/Climb 177.5/Cruise 177/Loiter 171	T.O. 183/Climb 177.5/Cruise 177/Loiter 170	T.O. 183/Climb 177.5/Cruise 177/Loiter 171
L/D	Climb 15.7/Cruise 15/Loiter 17.3	Climb 15.7/Cruise 15/Loiter 17.2	Climb 15.7/Cruise 15/Loiter 17.2	Climb 15.7/Cruise 15/Loiter 17.2
Fuselage length/ Diameter (m)	15.64/2.23	16.61/2.37	17.14/2.44	17.13/2.44
Wing span (m)/Area (m^2)	20.77/39.22	22.03/44.12	22.71/46.89	22.70/46.87
Batteries weight (kg)	–	650	864	861
Block fuel (kg)	928	733	782	729
Empty weight (kg)	4,250	4,692	4,935	4,989
MTOM (kg)	7,178	8,075	8,582	8,579
TOFL (m)	706	680	699	699
Block fuel reduction (%)	datum	−21.01%	−15.73%	−21.44%
CO2 reduction (%)	datum	−21.01%	−15.73%	−21.44%

to a slimmer block fuel reduction benefit of 15.73%. Finally, *Hybrid* 3 is sized, with the same specific energy as *Hybrid* 1, but with a higher H_p. As a result, the total amount of batteries increases, thus the operating empty mass and maximum take-off mass also increase. Therefore, the benefit of block fuel reduction increases to 21.44%. In conclusion, even though *Hybrid* 3 has a H_p of 45%, it provides only 0.43% more block fuel reduction than *Hybrid* 1, with a H_p of 35%, thus proving the impact of additional battery weight on the aircraft sizing "snowball effect".

3.5 Structural optimisation

The produced aircraft geometry from this framework is used to create the FEA structural model of the wing-box. An in-house script has been developed that enables parametric structural modeling of the aircraft, focusing on the wing. The initial structural model is imported in ANSA [53], to discretise the geometry into FE elements. The structural model of the wing-box consists of the main structural

https://doi.org/10.1017/aer.2022.32 Published online by Cambridge University Press

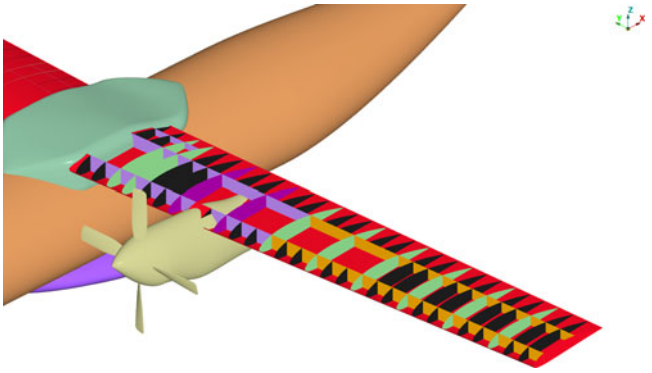

Figure 6. *Wing structure model.*

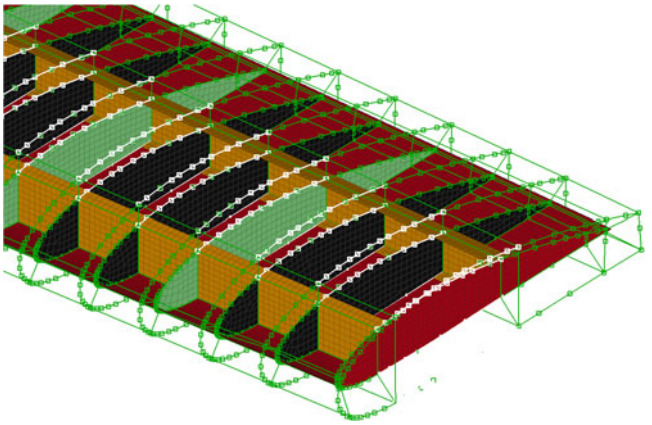

Figure 7. *Morph boxes definition.*

elements, i.e., spars and ribs, along with the exterior skin of the wing, as shown in Fig. 6. A point mass mounted on the frame is included to represent the engine assembly weight and volume elements are placed inside the wing-box to account for the available fuel and batteries storage.

The scope of the structural optimisation is to find the optimum spars position that minimises the root stresses and the maximum deflection of the structure, while the required battery and fuel storage volume inside the wing-box is a constraint. For this reason, morphing boxes were created, that enable the FE entities to alter their shape and position in the model, while ensuring that the elements stay attached to each other. The spars slide in the chord direction, altering the width of the wing-box, as shown in Fig. 7. The internal spar movement affects the total available volume for fuel and batteries storage, as well as the location of the wing centre of mass in the longitudinal direction. The exterior skin of the wing is used as a constraint and the spars slide on the wing skin, without affecting the external aerodynamic shape of the wing. The spar sliding on the wing skin alters their second moment of inertia, therefore the structure is strengthened or weakened, according to the spar movement. Additionally, the impact of the longitudinal movement of the centre of mass of the components stored inside the wing, as well as the wing itself, that occurs from the structural optimisation is examined in the positioning and stability module of the framework.

The structural model consists of 45,540 CQUAD4 and 656 CTRIA3 elements that represent the spars, ribs, and the exterior skin of the wing, whereas 12,000 CHEXA6 elements were used to model the available energy storage inside the wing-box. Load boundary conditions include gravity and lift

https://doi.org/10.1017/aer.2022.32 Published online by Cambridge University Press

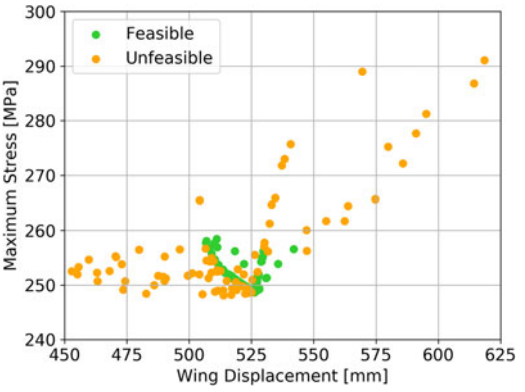

Figure 8. *Max stress vs max wing deformation design space for Hybrid 1 case.*

distributed as force on the exterior skin of the wing, using Schrenk's approximation on lift distribution [54], while the spars are supported on the wing root. The case of $2.5 \cdot g$ maneouver is tested at maximum take-off mass, as it results in the maximum bending moments on the wing structure. The solution is a static structural SOL 101. The optimisation case is set up in modeFRONTIER [55], using the Simplex algorithm. The objective function is to minimise the induced stresses at the root, with constraints in maximum wing deformation and minimum volume for fuel and battery storage.

The design space explored is shown in Fig. 8, including both feasible and unfeasible solutions. The x axis shows the maximum wing deformation, while the y axis represents the maximum stress on the root. Pairs of values for the spars position that satisfy all the constraints, i.e., the maximum wing deflection and available volume for batteries and fuel storage, are marked as feasible. Many spars positioning pairs lead to minimum root stresses and simultaneously lower wing deformations, however the volume criteria are not met. This means that a compromise between lower wing deflection and storage availability must be made. A more detailed design space exploration, with additional design variables, can be found in the work of Nasoulis et al. [56], for the investigation of the impact of the non-structural weight added on the stress, deformation and spanwise thickness distribution of the structure. Furthermore, correlations between wing deflection and storage volume, as well as component thickness and stresses are presented in the aforementioned work. In conclusion, the optimisation process results in an overall stress reduction of 41% for the root stresses and a 24.5% reduction of the total wing deformation, compared to the initial wing-box design, as derived from the model.

Stress results are shown in contour plot in Fig. 9. It is evident that there is a higher stress concentration at the root, as the wing is cantilever. Gray-scaled areas have minimum stresses; thus, topology optimisation can be applied for material reduction. In addition, although the root stresses are within acceptable limits [57], truss-bracing the wing will result in further stress relief, leading to significant weight reduction. However, both proposals belong to a later — more detailed — step of the aircraft design, thus they are beyond the scope of this work.

3.6 Positioning aspects and stability

Combining the component-wise weight estimation, the 3D sketch of the aircraft, and the position of the fuel and batteries storage compartments, the aircraft's total centre of mass can be calculated. The origin of the coordinate system used in this work is the fuselage's nose and each component is placed with reference to that point. A rule of thumb for the initial positioning of the wing is that the mean aerodynamic chord of the wing must be collinear with the aircraft centre of mass to ensure stability. In the stability evaluation process, the position of the wing can alter to fulfil the stability criteria. In addition, the empennage should be placed appropriately to generate the required moment to counteract the pitching

https://doi.org/10.1017/aer.2022.32 Published online by Cambridge University Press

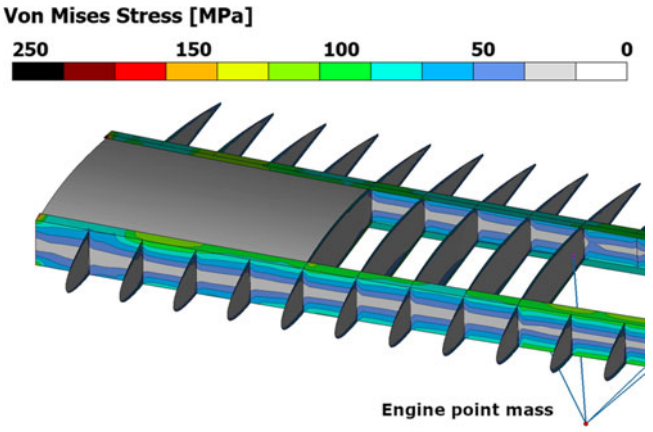

Figure 9. *Equivalent Von Mises stress contour plot on wing structure for Hybrid 1 case.*

motion of the aircraft. Finally, the positioning of the rest of the components is done with respect to the available volume for storage and maintenance practicality. In Table 8, the x location of each component is presented, along with the calculated mass. In an aircraft this size, the positioning of the batteries is of utmost importance, as the available storage space is generally restricted. It is evident that stability issues will raise if all the weight of batteries is concentrated in one specific compartment of the aircraft. One solution is to integrate the batteries inside the floor of the aircraft. This solution will result in a uniform weight distribution, that will not have a huge impact on stability. However extra insulation measures must be taken to protect the passengers in that case and practicality issues in maintenance will raise. An interesting approach can be found on the work of Riboldi et al. [58], where the batteries are part of the structural members of the aircraft. These structural batteries resemble the structure of carbon fiber composites, where the matrix has dielectric characteristics and can store electric energy, while maintaining the structural integrity. On the other hand, batteries can be split into different packages and placed in the fuselage in a way that they cancel each other out, to preserve stability. In that case the additional cable weight should be considered and, accessibility issues must be addressed, for repairing purposes. In the examined case, three batteries containers are selected that are placed in different segments, as shown in Table 8. The weight of the DC cables for the connection of these packs, is equally distributed in the three packs for the calculation of the centre of mass.

To retrieve the positioning values of the designed components, OpenVSP is used. By using cross-sections and assuming a uniform material distribution along the shape of each component, the centre of mass is extracted. The centre of mass of the batteries and fuel inside the wing-box is an output of the structural optimisation simulation. All things considered; the total aircraft centre of mass is evaluated. In Table 9 some basic aircraft loading conditions are examined, in order to find the most forward and most aft position of the centre of mass. Results presented in Tables 8, 9 are unique, since no similar references could be found in literature.

To calculate the static margin of the aircraft, the neutral point is required. In Equation (14), substituting $C_{m_{cg}} = 0$ and solving for $\bar{X}_{CoG}$ gives the neutral point. All aerodynamic coefficients appearing in Equation (14) are calculated in the Aerodynamics module. Static margin is calculated form Equation (15), using the most aft position of the centre of mass, as presented in Table 9, divided by the mean aerodynamic chord. The examined aircraft has a static margin of 24%, meaning a very stable aircraft. This leaves room for altering the positioning of the components, e.g., change the position of the electrical powertrain components to minimise cable length; an objective that will reduce the total electrical powertrain weight significantly. Furthermore, a 24% static margin indicates that an aft BLI engine can be integrated in this parallel-hybrid configuration, and reduce the required propulsion power up to 9%, considering the aero-propulsive benefit that it offers [59]. Adding an aft propulsion system with a total

https://doi.org/10.1017/aer.2022.32 Published online by Cambridge University Press

Table 8. *Component positioning and weight breakdown for Hybrid 1 case*

Component	X CoG loc. (m)	Mass (kg)	Moment (kg·m)
Main wing	7.60	675	5,132
Horizontal tail	15.51	50	776
Vertical tail	14.70	44	647
Fuselage	7.47	1,213	9,058
Forward landing gear	1.99	49	99
Main landing gear	7.67	280	2,110
Installed GTs	6.85	739	5,064
Electrical motors	6.85	107	733
Inverters	6.85	30	206
Cooling	11.57	62	718
EPS cables AC	6.85	18	123
EPS cables DC	∗incl. in bat.	54	–
Cabin	7.16	1,900	13,610
Cockpit	3.43	100	343
Battery pack 1	1.99	217	431
Battery pack 2	7.46	217	1,617
Battery pack 3	10.97	217	2,376
Fuel	7.85	733	5,755
Else	6.65	1,373	9,126

Table 9. *Aircraft loading scenarios for Hybrid 1 case*

Case	X CoG loc. (m)	Mass (kg)	Moment (kg·m)
1. Operating empty	7.225	5,342	38,596
2. Crew and no fuel	7.155	5,442	38,938
3. Crew and passengers with no fuel	7.157	7,342	52,547
4. Crew and fuel	7.238	6,175	44,695
5. Maximum take-off mass	7.220	8,075	58,302

mass of ≤240 kg will reduce static margin to 7%, which is still acceptable for a commuter aircraft.

$$C_{m_{cg}} = C_L \cdot (\bar{X}_{CoG} - \bar{X}_{acw}) + C_{mW} + C_{m_{w\delta_f}} \cdot \delta_f + C_{m_{fus}} - \frac{q_h \cdot S_h}{q \cdot S_W} \cdot C_{L_h} \cdot (\bar{X}_{ach} - \bar{X}_{CoG}) - T \cdot \frac{z_E}{q \cdot S_W \cdot \bar{c}} \quad (14)$$

$$S.M. = \bar{X}_{np} - \bar{X}_{CoG} \quad (15)$$

Subsequently, the trim analysis of the aircraft is conducted, using the most forward position of the centre of mass. The scope of this analysis is to ensure that the empennage can produce enough moment to counteract the pitching motion of the aircraft at all mission phases. Three key parameters affect the produced empennage moment, i.e., the horizontal tail reference area and incidence, and the longitudinal distance from the wing. These parameters can alter to ensure a well-trimmed design, with the most common parameter being the horizontal tail incidence angle. Using Equation (14) for various angles of attack the aim is to find the elevator deflection that results in zero moment coefficient. In Fig. 10, the trim plot for cruise is presented, with wing flap deflection set to zero. Results show, that for the lift coefficient required for cruise condition, the aircraft is trimmed for a zero-degree elevator deflection angle, with the horizontal tail incidence being -3 degrees. An overview of the examined disciplines in the proposed framework is presented in Fig. 11, combining aircraft sizing, geometry generation, structural

https://doi.org/10.1017/aer.2022.32 Published online by Cambridge University Press

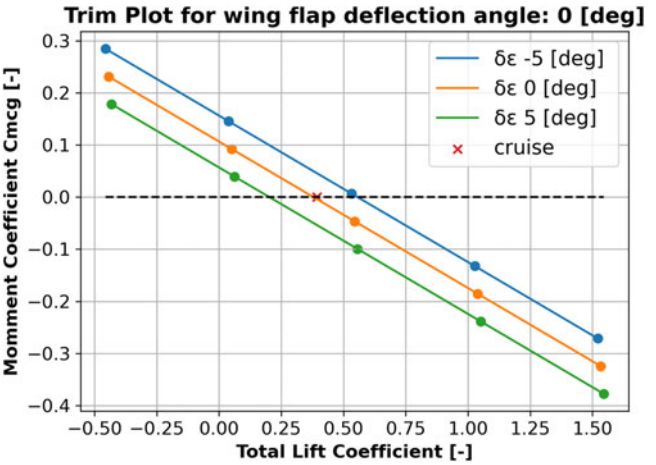

Figure 10. *Trim plot at cruise conditions for Hybrid 1 case.*

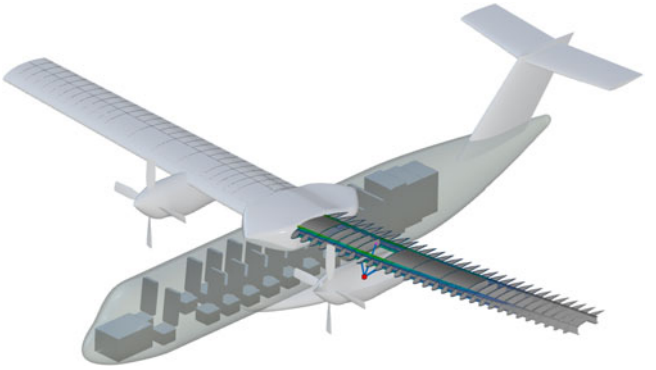

Figure 11. *Structural optimisation and positioning aspects for Hybrid 1 case.*

modeling and optimization of the wing box, and positioning aspects of the components that affect the static stability of the design.

4.0 Conclusions

An automated computational framework for the conceptual design of a hybrid-electric aircraft was presented and applied to the commuter class. Multiple disciplines were examined, including the aircraft sizing, aerodynamic behaviour, structural integrity, positioning, and static stability. The proposed framework was validated using data from four different conventional aircraft and weight prediction was within acceptable limits (<5%). A design space exploration was performed to determine the impact of battery specific energy and degree of hybridisation on maximum take-off mass. It was observed that energy-dense batteries (>800 Wh/kg) are required to have more than 15% of the total propulsion power derived from an electric source, while complying with the CS-23 airworthiness certification in terms of maximum take-off weight, for the parallel hybrid configuration. Three parallel hybrid-electric designs with different technological advancements per case, were compared to a reference aircraft with 2014 technology, to determine the benefit of electrification in terms of block fuel and CO_2 emissions reduction. Fuel economy increased with range, as the degree of hybridisation was set constant for the mission.

https://doi.org/10.1017/aer.2022.32 Published online by Cambridge University Press

Additionally, the energy density requirement for batteries was reduced when more efficient powertrain components were assumed. Subsequently, a conceptual design summary was presented, comparing three hybrid-electric aircraft variants to a conventional aircraft with 2014 technology. Results indicated that the block fuel reduction of *Hybrid* 1 was marginally lower than that of *Hybrid* 3, despite the latter having 10% more degree of hybridisation, thus proving the impact of the additional battery weight on the overall aircraft sizing. The structural optimisation of the wing-box suggested that trade-offs exist between wing deflection and storage availability for fuel and batteries inside the structure. The design was optimised to reduce the root stresses by altering the location of the spars, resulting in 41% stress reduction and 24.5% deflection reduction compared to the initial design. Finally, the impact of the components positioning on the static stability of the aircraft was examined, indicating that novel aircraft propulsion architectures, such as Boundary Layer Ingestion, can be applied to the commuter class. The addition of an aft BLI fan with a mass of 240 kg or less, led to a statically stable aircraft, with a 7% static margin.

Acknowledgments. Part of the work described in this article was done within the project HECARRUS, which has received funding from Clean Sky 2 Joint Undertaking (JU) under the European Union's Horizon 2020 Research and Innovation Programme under Grant Agreement number 865089. In addition, the authors would like to thank the project's Technical Advisory Board members, for their support and guidance. In addition, the authors would like to thank Alexandre Mugnai from ESTECO SpA for providing a free license for modeFRONTIER. Finally, the authors would like to thank Panagiotis Kouvrakis, George Korbetis and Eva Ioannou from BETA CAE SYSTEMS S.A. for the fruitful discussions and for helping with the optimisation part of this research.

References

[1] European Aviation Safety Agency (EASA), European aviation environmental report 2019, 2019, https://doi.org/10.2822/309946

[2] Epstein, A.h. and O'Flarity, S.M. Considerations for reducing aviation's co2 with aircraft electric propulsion, *J. Propul. Power*, 2019, **35**, (3), pp 572–582, https://doi.org/10.2514/1.B37015

[3] Henderson, R.P., Martins, J.R.R.A. and Perez, R.E. Aircraft conceptual design for optimal environmental performance, *Aeronaut. J.*, 2012, **116**, (1175), https://doi.org/10.1017/S000192400000659X

[4] Roskam, J. *Airplane Design Part I-VIII*, Roskam Aviation and Engineering Corp., 1985.

[5] Raymer, D.P. *Aircraft Design: A Conceptual Approach*, American Institute of Aeronautics and Astronautics - AIAA, 2018.

[6] Gudmundsson, S. *General Aviation Aircrafts Design: Applied Methods and Procedures*, Butterworth-Heinemann, 2014, Oxford, GB.

[7] Nicolai, L.M. and Carichner, G.E. *Fundamentals of Aircraft and Airship Design – Volume I – Aircraft Design*, AIAA, 2010, Reston, VA, USA.

[8] de Vries, R., Hoogreef, M.F.M. and Vos, R. Range equation for hybrid-electric aircraft with constant power split, *J. Aircraft-Eng. Note*, 2020, https://doi.org/10.2514/1.C035734

[9] Nam, T., Soban, D.S. and Mavris, D.N. *Power based sizing method for aircraft consuming unconventional energy, AIAA Aerospace Sciences Meeting and Exhibit*, AIAA, 2005.

[10] Finger, D.F., de Vries, R., Vos, R., Braun, C. and Bil, C. A comparison of hybrid-electric aircraft sizing methods, AIAA Scitech 2020 *Forum*, AIAA, 2020, https://doi.org/10.2514/6.2020-1006

[11] Finger, D.F., Braun, C. and Bil, C. Initial sizing methodology for hybrid-electric general aviation aircraft, *J. Aircraft*, 2019, https://doi.org/10.2514/1.C035428

[12] de Vries, R., Brown, M.T.H. and Vos, R. Preliminary sizing method for hybrid-electric distributed-propulsion aircraft, *J. Aircraft*, **56**(6), https://doi.org/10.2514/1.C035388

[13] Orefice, F., Nicolosi, P., Della Vecchia, P. and Ciliberti D. Conceptual design of commuter aircraft including distributed electric propulsion, AIAA Aviation *Forum*, AIAA, 2020, https://doi.org/10.2514/6.2020-2627

[14] Trainelli, L., Riboldi, C.E.D., Salucci, F. and Rolando, A. A general preliminary sizing procedure for pure-electric and hybrid-electric airplanes, CEAS Conference, 2020.

[15] European Aviation Safety Agency (EASA). Easy access rules for normal-category aeroplanes (cs-23), cs amendment 5, amc/gm issue 2, 2019, https://www.easa.europa.eu/downloads/106158/en

[16] Federal Aviation Administration (FAA). Electronic code of federal regulations: Part 23 – airworthiness standards: Normal category airplanes, 2016, https://www.ecfr.gov/current/title-14/part-23

[17] Kruger, M. and Uranga A. The feasibility of electric propulsion for commuter aircraft, AIAA Scitech 2020 *Forum*, AIAA, 2020, https://doi.org/10.2514/6.2020-1499

18] Fefermann, Y., Maury, C., Zarati, K., Salanne, J.P., Pornet, C., Thoraval, B. and Isikveren, A. Hybrid-electric motive power systems for commuter transport applications, 30th ICAS Conference, Daejeon, South Korea, 2016.

[19] European Aviation Safety Agency (EASA) Certification Specifications and Acceptable Means of Compliance for Large Aeroplanes (CS-25), Amendment 27, https://www.easa.europa.eu/downloads/134259/en

[20] Gkoutzamanis, V.G., Kavvalos, M.D., Srinivas, A., Mavroudi, D., Korbetis, G., Kyprianidis, K.G. and Kalfas, A.I. Conceptual design and energy storage positioning aspects for a hybrid-electric light aircraft, *J. Eng. Gas Turbines Power*, 2021, **143**, (9), https://doi.org/10.1115/1.4050870

[21] Gesel, H., Wolters, F. and Plohr, M. System analysis of turbo-electric and hybrid-electric propulsion systems on a regional aircraft, *Aeronaut. J.*, 2019, **123**, (1268), https://doi.org/10.1017/aer.2019.61

[22] Juretzko, P.G., Immer, M. and Wildi, J. Performance analysis of a hybrid-electric retrofit of a ruag dornier do 228ng, *CEAS Aeronaut. J.*, 2019, https://doi.org/10.1007/s13272-019-00420-2

[23] Wall, T.J. and Meyer, R.T. Hybrid electric aircraft switched model optimal control, *J. Propul. Power*, 2020, **36**, (4), pp 488–497, https://doi.org/10.2514/1.B37419

[24] HECARRUS Project, 865089. Efficiency and TRL of each component of the powertrain, 2020, https://cordis.europa.eu/project/id/865089/results

[25] Bodson, M., Sadey, D.J., Hunker, K.R., Theman, C.J., Taylor, L.M. and Csank, J.T. Hybrid electric propulsion using doubly fed induction machines, *J. Propul. Power*, 2020, **36**, (1), pp 78–87, https://doi.org/10.2514/1.B37415

[26] Emrax Emrax 348 technical data table, 2019, https://emrax.com/wp-content/uploads/2020/03/manual_for_emrax_motors_version_5.4.pdf (Accessed: 16-Feb-2022)

[27] Marrufo, M. and Kloesel, K. X-57 60kw permanent magnet synchronous cruise motor finite element electromagnetic modeling, 2019, https://ntrs.nasa.gov/citations/20190033258

[28] Siemens, A.G. eaircraft: Hybrid-elektrische antriebe fur luftfahrzeuge, 2019, https://www.bbaa.de/fileadmin/user_upload/02-preis/02-02-preistraeger/newsletter-2019/02-2019-09/02_Siemens_Anton.pdf (Accessed: 16-Feb-2022)

[29] MagniX. 2019, https://magnix.aero/services (Accessed: 16-Feb-2022)

[30] Bradley, M.K. and Droney, C.K. Subsonic ultra green aircraft research: Phase i final report, NASA Tech, 2011, https://ntrs.nasa.gov/api/citations/20110011321/downloads/20110011321.pdf

[31] Jansen, R., Kascak, P.E., Dyson, R.W., Woodworth, A., et al. High efficiency megawatt motor preliminary design, AIAA Propulsion and Energy 2019 *Forum*, 2019, https://doi.org/10.2514/6.2019-4513

[32] NASA Glenn Research Centre. Ohio state university induction machine, in *Advanced Superconducting Motor Experimental Demonstrator* ASuMED Project, 2017, [Online]. Available: http://asumed.oswald.de, https://www1.grc.nasa.gov/aeronautics/eap/technology/electric-machines/induction-machine/ (Accessed: 16-Feb-2022)

[33] Wang, Y., Nuzzo, S., Zhang, h., Zhao, W., Gerada, C. and Galea, M. Challenges and opportunities for wound field synchronous generators in future more electric aircraft, *IEEE Trans. Transp. Electrif.*, 2020, https://doi.org/10.1109/TTE.2020.2980189

[34] Yoon, A., Yi, X., Martin, J., Chen, Y. and Haran, K. A high-speed, high-frequency, air-core pm machine for aircraft application, IEEE Power Energy Conference, https://doi.org/10.1109/PECI.2016.7459221

[35] Sivasubramaniam, K., Zhang, T., Lokhandwalla, M., Laskaris, E.T., Bray, J.W., Gerstler, B., Shah, M.R. and Alexander, J.P. Development of a high speed hts generator for airborne applications, *IEEE Trans. Appl. Supercond.*, 2009, 19, (3), pp 1656–1661, https://doi.org/10.1109/TASC.2009.2017758

[36] National Aeronautics and Space Administration (NASA). 2012, https://www.nasa.gov/directorates/heo/scan/engineering/technology/txt_accordion1.html (Accessed: 16-Feb-2022)

[37] Romano, D.G., Apuleo, G. and Duda, J. Affordable and environmental friendly small commuter aircraft improving european mobility, *Int. J. Aerospace Mech. Eng.*, 2020, **14**, (9), pp 329–337

[38] European Aviation Safety Agency (EASA) Type-certificate data sheet for pt6a-67 series models, 2019, https://www.easa.europa.eu/downloads/7787/en

[39] McDonald, R.A. and Gloudemans, J.R. Open vehicle sketch pad: An open source parametric geometry and analysis tool for conceptual aircraft design, AIAA 2022-0004, AIAA SCITECH 2022 *Forum*, 2022, https://doi.org/10.2514/6.2022-0004

[40] Teichel, S.H., Dörbaum, M., Misir, O., Merkert, A., Mertens, A., Seume, J.R. and Ponick, B. Design considerations for the components of electrically powered active high-lift systems in civil aircraft, *CEAS Aeronaut. J.*, 2015, **6**, (1), pp 49–67.

[41] Staton, R. *Cargo/Transport Statistical Weight Estimation Equations*, Vought Aircraft, Rept. 2-59320/9R-50549, 1969.

[42] Jackson, A. *Preliminary Design Weight Estimation Program*. Aero-Commander Div. Rept. 511-009, 1971.

[43] FlightSafety International. Beech 1900 Airliner Pilot Training Manual, 2000

[44] Giannakakis, P., Laskaridis, P., Nikolaidis, T. and Kalfas, A.I. Toward a scalable propeller performance map, *Journal of Propulsion and Power*, 2015, **31**, (4), https://doi.org/10.2514/1.B35498

[45] Zhang, D., He, J. and Pan D. A megawatt-scale medium-voltage high-efficiency high power density 'sic+ si' hybrid three-level anpc inverter for aircraft hybrid-electric propulsion systems, *IEEE Trans. Ind. Appl.*, 2019, 55, (6), pp 5971–5980, https://doi.org/10.1109/ECCE.2018.8558199

[46] Vratny, P.C., Gologan, C., Pornet, C., Isikveren, A. and Hornung, M. Battery pack modeling methods for Universally-Electric Aircraft, 4th CEAS Air and Space Conference, Sweden, 2013

[47] RUAG Aerospace Services GMBH. Dornier 228 Advanced Commuter Facts and Figures, 2014, https://ruag-international.picturepark.com/v/SQmZwhjP/ (Accessed: 3-Feb-2022)

[48] ATR CM Marketing, ATR 42-600 Design Specsheet, 2015, https://skybrary.aero/sites/default/files/bookshelf/3695.pdf (Accessed: 16-Feb-2022)

[49] 328 Support Services GmbH. Dornier 328-100 TP Design Specsheet, 2013 https://328.eu/wp-content/uploads/2013/06/328-100-turboprop.pdf (Accessed: 16-Feb-2022)

[50] General Electric Aviation, Ge aviation press release, 2018 https://www.geaviation.com/press-release/business-general-aviation/catalysttm-engine-certification-testing-about-begin (Accessed: 13-Feb-2022).

https://doi.org/10.1017/aer.2022.32 Published online by Cambridge University Press

[51] Nasoulis, C.P., Protopapadakis, G., Gkoutzamanis, V.G. and Kalfas, A.I. The impact of propulsive architecture on the design of a 19-passenger hybrid-electric aircraft, *IOP Conference Series: Materials Science and Engineering*, vol. **1226**, 2022, https://doi.org/10.1088/1757-899x/1226/1/012074
[52] Schiphol airport, The Netherlands. Website: https://www.schiphol.nl/en/schiphol-as-a-neighbour/page/emission-free-by-2030/ (Accessed: 16-Feb-2022)
[53] BETA CAE Systems AG. Ansa - the advanced pre-processing software for complete model build-up, 2018, https://www.beta-cae.com/brochure/ansa_brochure.pdf (Accessed: 16-Feb-2022)
[54] Schrenk, O. A simple approximation method for obtaining the spanwise lift distribution, 1940.
[55] ESTECO SpA. https://www.esteco.com/modefrontier (Accessed: 16-Feb-2022)
[56] Nasoulis, C.P., Tsirikoglou, P. and Kalfas, A.I. Structural optimisation of the wing-box for a hybrid-electric commuter aircraft, Accepted for publication at the Proceedings of Global Propulsion and Power Society, GPPS Xi'an21, April 2022.
[57] Torenbeek, E. *Advanced Aircraft Design: Conceptual Design, Technology and Optimisation of Subsonic Civil Airplanes*, John Wiley & Sons, 2013.
[58] Riboldi, C.E.D., Trainelli, L. and Biondani, F. Structural batteries in aviation: A preliminary sizing methodology, *J. Aerospace Eng.*, 2020, 33, https://doi.org/10.1061/(ASCE)AS.1943-5525.0001144
[59] Hall, D.K., Huang, A.C., Uranga, A., Greitzer, E.M., Drela, N. and Sato, S. Boundary layer ingestion propulsion benefit for transport aircraft, *J. Propul. Power*, 2017, **33**, (5), pp 1118–1129, https://doi.org/10.2514/1.B36321

Cite this article: Nasoulis C.P., Gkoutzamanis V.G. and Kalfas A.I. (2022). Multidisciplinary conceptual design for a hybrid-electric commuter aircraft. *The Aeronautical Journal*, **126**, 1242–1264. https://doi.org/10.1017/aer.2022.32